ELSEVIER

Journal of Nuclear Materials 282 (2000) 131–136

journal of nuclear materials

www.elsevier.nl/locate/jnucmat

Helium and hydrogen induced hardening in 316LN stainless steel

J.D. Hunn *, E.H. Lee, T.S. Byun, L.K. Mansur

Metals and Ceramics Division, Oak Ridge National Laboratory, P.O. Box 2008, Oak Ridge, TN 37831-6151, USA

Received 3 May 2000; accepted 15 September 2000

Abstract

In certain radiation environments, such as the spallation neutron source (SNS) presently in design and construction, the high transmutation production rate for helium and hydrogen, concomitant with displacement damage, may affect the mechanical properties of structural materials. To better understand this effect, we have studied type 316LN stainless steel specimens implanted with medium energy Fe-, He-, and H-ions, alone and in combination. In this report, we present nanoindentation measurements of the incremental increase in hardness caused by 360 keV He-ions implanted at 200°C to concentrations from 2 to 200 000 appm. The He-induced hardening was found to saturate at twice the level measured for Fe-induced displacement damage alone. The additional hardening at high helium concentrations was associated with the presence of helium filled cavities (bubbles), observed by transmission electron microscopy (TEM). We also found that co-injection of helium and hydrogen resulted in more hardening than was observed for He-implantation alone.

PACS: 61.82.Bg

1. Introduction

The production of helium by nuclear transmutation in components of nuclear power reactors has been recognized for some time to lead to detrimental effects on the material properties [1]. Because of its low solubility in metals, interstitial helium atoms produced by transmutation or implantation rapidly precipitate out at nearby sinks (vacancies, vacancy complexes, and grain boundaries), where they are strongly trapped [2,3]. As He-atom clusters grow, they eventually eject lattice atoms to form cavities. Estimates made from the size and number density of these cavities yield helium bubble pressures of several GPa [4]. The stabilization of cavities by helium, resulting in void swelling, has been reported at temperatures from 350°C to 700°C [5]. In the spallation neutron source (SNS), helium will be generated at transmutation rates of up to 200 appm/dpa, 20 times that predicted for the first wall in a fusion reactor. In addition, as much as 1000 appm/dpa of hydrogen is expected. Recent triple ion beam irradiation studies of radiation damage effects at SNS target vessel conditions have shown a contribution of both helium and hydrogen to hardening in austenitic and ferritic steels irradiated between 25°C and 200°C [6–8].

In order to better understand the effect of helium build up in the SNS target vessel, type 316LN stainless steel specimens were systematically implanted with helium to concentrations ranging from 2 to 200 000 appm. The corresponding displacement damage ranged from 10^{-4} to 15 dpa. To separate the contribution of the displacement damage from that of the helium impurity, a second set of specimens was implanted with Fe-ions to produce a similar displacement profile over the same dose range but with negligible change to the alloy composition. Specimens were then studied by nanoindentation and transmission electron microscopy (TEM). The additional contribution of hydrogen to hardening and microstructure, expected from a recent study of deuterium trapping [9], was also investigated.

* Corresponding author. Tel.: +1-865 574 2480; fax: +1-865 574 0641.

E-mail address: hunnjd@ornl.gov (J.D. Hunn).

0022-3115/00/$ - see front matter
PII: S0022-3115(00)00424-4

2. Experimental

An AISI 316LN stainless steel was obtained from Jessop Steel Company with specific composition (in wt%) 0.009 C, 1.75 Mn, 0.029 P, 0.002 S, 0.39 Si, 16.31 Cr, 10.2 Ni, 2.07 Mo, 0.16 Co, 0.23 Cu, 0.11 N, balance Fe (heat 18474). This was rolled and cut into 3 mm discs followed by a solution anneal at 1050°C for 2 h. The surface of the discs were mechanically polished to 0.1 μm followed by a final electropolish to remove the work hardened surface. Irradiations were carried out at the Oak Ridge National Laboratory's Triple Ion Facility [10]. Specimen temperature was controlled and monitored throughout the irradiation. For this study, specimens were irradiated at 30°C and 200°C. Ion beams were defocused to provide a uniform flux profile across the specimen and, in the case of multiple ion implants, were simultaneously injected using separate Van de Graaff accelerators. He and Fe ions were injected at an angle of 15° from the surface normal, necessitated by the relative positions of the three accelerators. H and D ions were injected at 0° to the normal. Fluence was constantly monitored and beam currents were controlled to maintain a uniform relative flux during the multiple implants.

The computer code SRIM-98 [11] with the modified Kinchen–Pease approximation was used to calculate the initial ion and defect distributions. Appropriate ion energies were selected in order to produce an overlap of the depth profiles, with a peak around 800 nm below the surface. The 800 nm depth was selected on the basis of available ion energy and to maximize ion-beam-analysis sensitivity, while being sufficiently deep to minimize surface effects [12,13]. For dual H/He implants, a relative H:He concentration of 5:1 was maintained. This injection ratio was appropriate to predicted transmutation rates under SNS target vessel conditions. Initial damage distributions were calculated in terms of displacements per atom (dpa) using the NRT formula [14],

$$\mathrm{dpa} = \frac{0.8}{2E_\mathrm{d}}\left(\frac{\mathrm{d}E}{\mathrm{d}x}\right)_n \frac{\mathrm{fluence}}{\mathrm{density}}. \quad (1)$$

Here, $E_\mathrm{d} = 40$ eV is the energy to displace an atom out of its site in the lattice and $(\mathrm{d}E/\mathrm{d}x)_n$ is the linear energy transferred (LET) per ion to the target by nuclear processes. In SRIM, $(\mathrm{d}E/\mathrm{d}x)_n$ equals the sum of the phonon and binding energy distribution profiles (the binding energy profile is obtained from the SRIM vacancy profile by multiplying by the lattice binding energy). Table 1 lists the calculated values for the various ions implanted in this study. In this table, the ion and displacement damage profiles are presented by reporting the position of the peak in the distribution along with the positive and negative distance from this peak to the position where the profile has dropped off by 50%. The non-symmetry in these 'half' widths indicates the tendency of the distribution to be skewed toward the irradiated surface. An average ion concentration about the peak was calculated by taking the average between these two 'half' widths (this average included about two thirds of the implanted ions). An average displacement damage was calculated between 700 and 900 nm, which is roughly the range in which the individual ion concentrations were averaged and is also the region that was observed by TEM analysis as described below.

At the moderate implant temperatures used, the final He-concentration profile was expected to be essentially equivalent to the initial profile as calculated by SRIM, with perhaps a slight broadening at the higher fluences [4,15]. The absence of any appreciable long range diffusion of helium is due to its negligible solubility and high detrapping energy [2,16]. Hydrogen, on the other hand, exhibits a much higher (though still endothermic) solubility in stainless steel accompanied by a relatively low binding energy to simple lattice defects [3,17]. In specimens implanted with hydrogen alone, H will quickly diffuse away from the implanted area at moderate temperatures. Below 100°C, some hydrogen is weakly trapped by radiation-induced defects, in a depth

Table 1
Irradiation profiles as calculated by SRIM [11][a]

Ion energy and species	Peak of ion profile (nm)	Position of half max in ion profile relative to peak	Average ion concentration between half max points (per 10^{15} ions/cm^2) (appm)	Peak of damage profile (nm)	Position of half max in damage profile relative to peak	Average displacement damage between 700 and 900 nm (per 10^{15} ions/cm^2) (dpa)
180 keV H	785	−80 nm, +60 nm	567	755	−110 nm, +70 nm	0.0033
150 keV D	785	−120 nm, +90 nm	385	740	−170 nm, +110 nm	0.0067
360 keV He[b]	805	−150 nm, +100 nm	332	740	−180 nm, +120 nm	0.026
3500 keV Fe[a]	965	−190 nm, +130 nm	260	810	−450 nm, +200 nm	1.0

[a] Non-symmetric 'half' widths about the peaks reflect skewing toward the irradiated surface. Energies were chosen such that the H, D, and He ion profiles overlapped the Fe-induced displacement profile.
[b] He and Fe profiles are calculated for 15° off of normal to reflect Triple Ion Facility configuration.

profile greatly broadened and reduced from the calculated initial profile. Above this temperature, negligible hydrogen retention has been measured for 316LN implanted by hydrogen alone [9]. However, under co-implantation with helium, hydrogen is strongly trapped by the He-clusters. For room temperature co-implantation of D and He at the energies listed in Table 1, we have measured by nuclear reaction analysis that ≃60% of the injected deuterium was retained in a depth profile replicating the calculated initial He-profile [9]. At 200°C, this retention dropped to ≃10%.

After irradiation, the relative hardening in the implanted region was measured using Nano Instrument's Nano Indenter II. The nanoindentation method [18] consisted of supplying a constantly increasing load to a pyramidal Berkovich diamond indenter tip. The load was recorded as a function of indenter depth. Simultaneously, the stiffness as a function of depth was recorded using a dynamic lock-in technique. The hardness as a function of contact depth is defined as the load at that depth divided by the contact area of plastic displacement. The contact depth of plastic deformation can be calculated from the indenter depth by using the measured stiffness at that depth to subtract out the elastic component. The contact area as a function of contact depth is a calibrated parameter and a function of the indenter tip geometry. Because the irradiation profiles were not constant as a function of depth and the stress field from the indenter extends about seven times the contact depth [19], it must be noted that the measured hardness values as a function of depth did not represent the actual hardness of the material at that depth. Nevertheless, because the shape of the irradiation profile remains consistent for a given ion species and energy, it is reasonable to use the nanoindentation measurements to compare the relative effect of irradiation fluence on hardening.

Fig. 1 shows the hardness versus depth for a typical indent. For contact depths less than 100 nm, hardness values were unreliable due to uncertainty in the indenter geometry and surface effects such as thin oxide films or polishing defects. At a depth of 700 nm, corresponding to the peak in the helium profile, the measured hardness was dominated by the large volume of softer unirradiated material beyond the implant range. A peak in the hardness occurred around 150 nm. At this depth, surface effects were reduced and the indenter was mostly sampling the implanted region. In comparing the relative hardening among specimens, the percent hardening with respect to virgin material was therefore calculated from the measured hardness at 150 nm contact depth.

The values of hardening in this report were typically obtained by averaging five individual indents on each of three separate specimens implanted under the same conditions. Scatter between the indents was on the order of ±1–2%. Care was taken to avoid areas on the surface

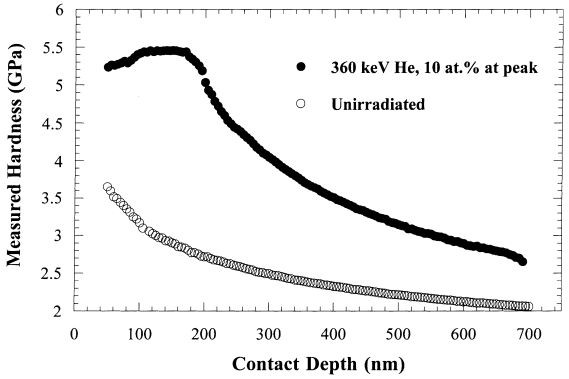

Fig. 1. Typical hardness profile for this work, as measured by nanoindentation technique. The peak at 150 nm contact depth corresponded to a peak at 800 nm in the actual hardness profile.

where pitting, mechanical defects, or impurities could be seen. Occasionally, an individual indent would result in a hardness versus depth curve well outside the average magnitude or of unusual shape. This was most likely due to subsurface precipitates or, in some cases, a simple failure in that particular indentation process. Such anomalous indents were not included in the averaging.

As already mentioned, the measured hardness at 150 nm contact depth was dependent on the depth profile of the hardness inducing defects. Ion energies were chosen such that the Fe-damage profile and final He-ion distribution profile were similar (see Table 1). Nevertheless, some additional uncertainty exists when comparing the relative hardening between the He- and Fe-irradiations.

After nanoindentation, one specimen for each irradiation condition was prepared for TEM analysis. This was done by removing the top ≃700 nm from the implanted surface and then back-thinning from the unirradiated side until perforation. TEM was performed on a Phillips CM-12 at 120 keV. Details of the TEM analysis and discussion of the microstructural evolution has been reported in a separate paper [20].

3. Results and discussion

Fig. 2 shows the measured hardening as a function of dose from 0.001 to 50 dpa for specimens irradiated at 200°C with 3.5 MeV Fe ions. The hardening increased rapidly at low dose, with a saturation beginning around 1 dpa. At the higher doses, the hardening reached a saturation level of ≃50% above the unirradiated hardness. TEM analysis [20] showed that the initial hardening increase was due to an increase in the density of 'black dot defects' (vacancy and interstitial clusters), which act as barriers to dislocation motion. The observed

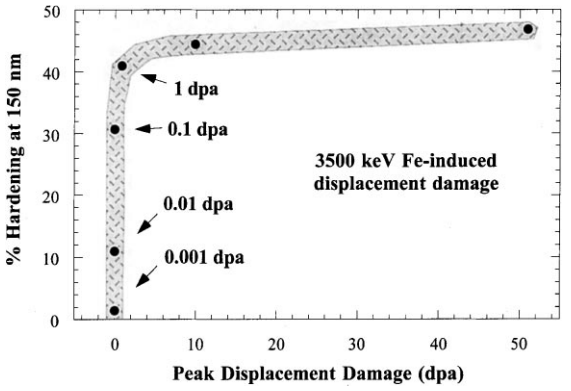

Fig. 2. Percent hardening at 150 nm contact depth versus radiation damage dose for 316LN irradiated with 3500 keV Fe at 200°C. Shaded line shows trend and estimates scatter in data. Hardening saturated at high dose.

saturation in hardening was consistent with a saturation in the black dot density around 1 dpa.

In contrast to the hardening due to Fe-irradiation, hardening in the He-injected specimens resulted from two separate pinning centers: radiation-induced defect clusters and helium filled cavities [21]. Fig. 3 compares the Fe-induced hardening from the previous figure with the hardening observed in specimens irradiated from 0.001 to 15 dpa using 360 keV He ions. This corresponded to an injected peak concentration of 2 to 200 000 appm. At low dose, the He-induced hardening was less than that observed for equivalent radiation damage from the more massive Fe-ion. This was due to a slower evolution of black dot defects, which has been explained in detail in a previous paper [20]. At higher fluence, the hardening in the He-injected specimens increased well beyond that observed for those irradiated with Fe-ions. The hardness saturated at 10–20 at.% He. Beyond this concentration, the amount of trapped gas was sufficient to cause the surface to blister and exfoliate. Helium induced blistering and its mechanisms have been studied in depth [22,23]. Wilson [24] reports a semi-empirical formula for the near surface He-concentration at which blistering occurs in metals as a function of temperature (in Kelvin),

$$C_{\mathrm{He}} = 0.5 - (T/T_{\mathrm{m}}), \tag{2}$$

where T_{m} is the absolute melting temperature. This predicts a critical concentration of 22%, in agreement with our results.

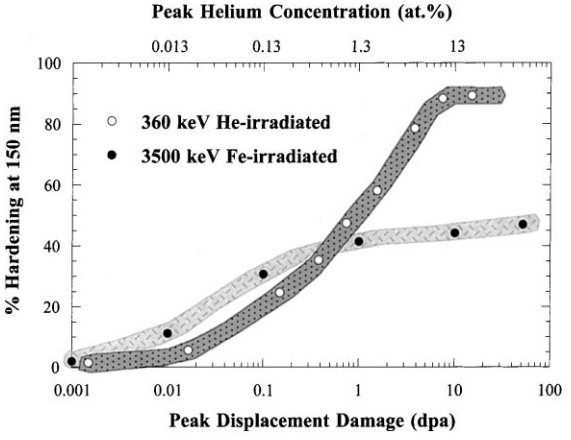

Fig. 3. Comparison of the percent hardening versus dose for 316LN irradiated with either He- or Fe-ions at 200°C. Top axis refers to solid circles only. Shaded lines show trends and estimate scatter in data. Above 1 at.%, He gas effects became evident.

Fig. 3 shows that the hardening in the He-irradiated specimens cannot be explained by displacement damage alone. Clearly, the presence of helium is dominating the hardening at the higher concentrations. TEM micrographs of specimens over a range of He-concentration are shown in Fig. 4. Above 5 at.%, bubbles could be clearly imaged and verified by over- and under-focused contrast. Between 1 and 5 at.%, bubble like features were observed, but individual bubbles could not be imaged. However, a comparison of micrographs as a function of the concentration decreasing in small steps, led to the conclusion that, in this range, bubbles were still present just beyond the resolution of the TEM analysis. Below 1 at.%, any bubble features were invisible to TEM.

The helium bubbles may affect the hardness in two ways. In addition to presenting a direct barrier to dislocation motion, we observed that the implanted helium acted to pin the (1 1 1)-type faulted Frank loops created by displacement damage. In contrast, for specimens implanted with Fe-ions alone, a significant fraction of these sessile faulted loops unfault to glissile (1 1 0)-type perfect loops, which present a lower barrier to dislocation motion.

A comment should be made concerning the rates of introduction of helium, hydrogen, and displacement damage. Because of the large range in fluence covered in this study (see Fig. 2) it was not experimentally feasible to maintain a constant flux throughout the He- or Fe-irradiations. The experimental dose rates ranged from 6×10^{-5} to 3×10^{-3} dpa/s for Fe-irradiation and 2×10^{-6} to 2×10^{-4} dpa/s for helium, with a corresponding He-ion injection rate of 0.02–2 appm/s. In comparison, the SNS is expected to operate at a time averaged damage rate of 10^{-6} dpa/s and, more significantly, with an instantaneous damage rate of 10^{-2} dpa/s and up to 2 appm He/s, during the proton pulse. It is known that radiation damage accumulates differently under different damage rates. A theoretical method has been developed to quantify this effect based on the concept of irradiation variable shifts [25]. In this

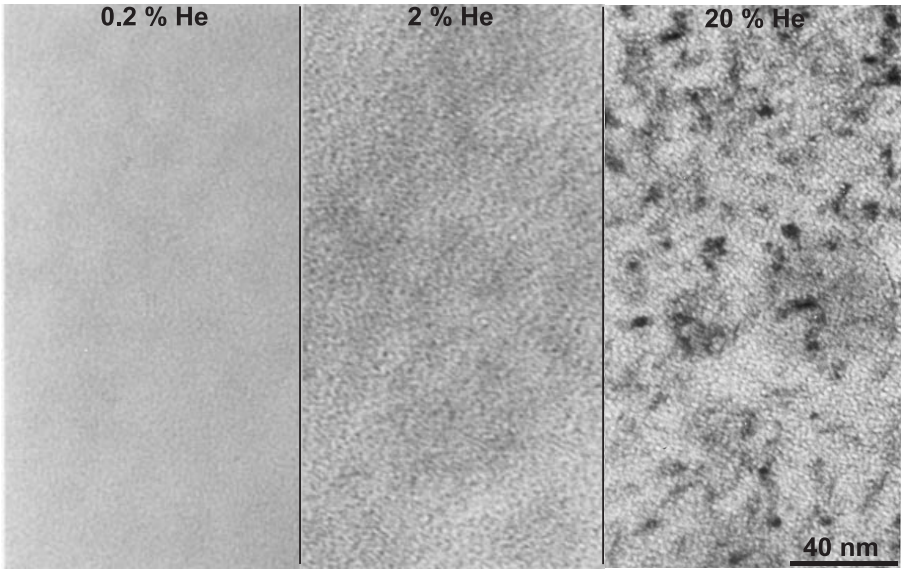

Fig. 4. TEM micrographs from a layer 700 to 800 nm below the original surface of 316LN specimens irradiated with 360 keV He at 200°C.

concept, a dependent irradiation variable, such as the cumulative number of point defects lost by mutual recombination, can be held invariant under a change in dose rate by varying a second independent variable, such as temperature. However, in the recombination dominant regime (high dose rate and low temperature) within which the present experiments fall, we expect the irradiation variable shifts to be small and we did not attempt to apply such corrections in comparing the results as a function of dose.

In irradiation conditions that involve the creation of both helium and hydrogen transmutation products, the trapping of hydrogen by helium clusters may present further concern by exacerbating the effect of gas bubble induced hardening. Fig. 5 shows the additional hardening that resulted from co-injection of hydrogen at room temperature. A definite systematic increase in hardening was observed, due to the implanted hydrogen. As mentioned above, we expected that ≃60% of the injected hydrogen would be trapped in or around the helium bubbles. Given the 5:1 fluence ratio of the co-implantation, this should result in 300% more trapped atoms than for helium implantation alone. However, the additional hardening from trapped hydrogen was equivalent to what would be observed for only 50% more helium atoms.

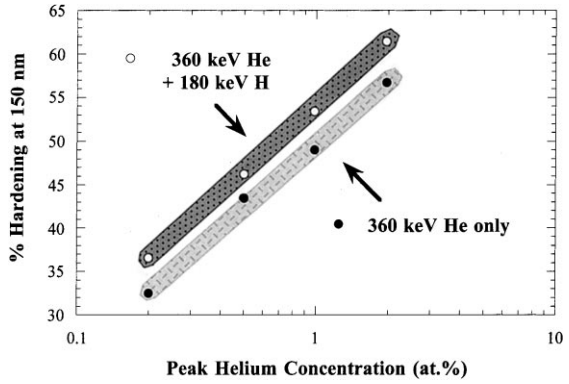

Fig. 5. Percent hardening at 150 nm contact depth versus He-concentration for specimens implanted at 30°C with He only (solid circles) and those co-implanted with an additional amount of H at a 5:1 ratio (open circles). Shaded lines show trends and estimate scatter in data. Additional hardening from the extra hydrogen is evident (vertical projection), but the additional hydrogen does not produce as much hardening as would the same amount of additional helium (horizontal projection).

4. Conclusion

Type 316LN stainless steel specimens were irradiated with either Fe-, He-, or He-plus H-ions. Hardening from Fe-ion-induced displacement damage was found to saturate around 10 dpa, but with a rapid onset, reaching half the saturated value at less than 0.1 dpa. At approximately 1 at.% helium concentration, dislocation and loop pinning by helium filled cavities in the lattice became significant. A hardening saturation value of almost twice that observed for displacement damage alone was reached at ≃20 at.% He, just shy of the critical

concentration for exfoliation. Hydrogen trapping by co-implanted helium produced additional hardening, but at a lower effective rate per H-atom than per He-atom.

For an SNS relevant transmutation rate of 200 appm He/dpa, 1 at.% helium corresponds to 50 dpa, a level five to ten times higher than the expected changeout interval of the target vessel. Therefore, the hardening in the SNS target vessel is expected to be dominated by displacement damage mechanisms throughout its design lifetime. Further effects of He and H on fracture processes, in addition to their effects on hardening, are also under investigation.

Acknowledgements

This research was sponsored by the Division of Materials Sciences, US Department of Energy, under contract No. DE-AC05-00OR22725 with UT-Battelle, LLC. We would like to thank S.W. Cook for assistance with irradiations and Drs M.B. Lewis and R.E. Stoller for technical review of the manuscript.

References

[1] L.K. Mansur, E.H. Lee, P.J. Maziasz, A.P. Rowcliffe, J. Nucl. Mater. 141–143 (1986) 633.
[2] E.V. Kornelsen, Radiat. Eff. 18 (1972) 227.
[3] K.L. Wilson, in: Data Compendium for Plasma–Surface Interactions, Nuclear Fusion Special Issue 1984, International Atomic Energy Agency, Vienna, 1984, pp. 28–42.
[4] P. Wang, Y. Li, J. Liu, G. Zhang, R. Ma, P. Zhu, C. Qiu, T. Xu, J. Nucl. Mater. 169 (1989) 167.
[5] L.K. Mansur, J. Nucl. Mater. 216 (1994) 101.
[6] E.H. Lee, G.R. Rao, J.D. Hunn, P.M. Rice, M.B. Lewis, S.W. Cook, K. Farrell, L.K. Mansur, in: M.S. Wechsler, L.K. Mansur, C.L. Snead, W.F. Sommer (Eds.), Materials for Spallation Neutron Sources, TMS, Warrendale, PA, 1998, p. 57.
[7] E.H. Lee, J.D. Hunn, G.R. Rao, L.K. Mansur, J. Nucl. Mater. 272 (1999) 385.
[8] E.H. Lee, J.D. Hunn, N. Hashimoto, L.K. Mansur, J. Nucl. Mater. 278 (2000) 266.
[9] J.D. Hunn, M.B. Lewis, E.H. Lee, in: AccApp 98 – Proceedings of the Second International Topical Meeting on Nuclear Applications of Accelerator Technology, American Nuclear Society, La Grange Park, 1998, p. 375.
[10] M.B. Lewis, W.R. Allen, R.A. Buhl, N.H. Packan, S.W. Cook, L.K. Mansur, Nucl. Instrum. and Meth. B 43 (1989) 243.
[11] J.F. Ziegler, J.P. Biersack, U. Littmark, The Stopping and Ranges of Ions in Solids, Pergamon, New York, 1985.
[12] L.K. Mansur, A.D. Brailsford, W.A. Coghlan, Acta Metall. 33 (1985) 1420.
[13] L.K. Mansur, M.H. Yoo, J. Nucl. Mater. 85&86 (1979) 529.
[14] M.J. Norgett, M.T. Robinson, I.M. Torrens, Nucl. Eng. Design 33 (1975) 50.
[15] M.B. Lewis, K. Farrell, Nucl. Instrum. and Meth. B 16 (1986) 163.
[16] M.B. Lewis, J. Nucl. Mater. 149 (1987) 143.
[17] M.B. Lewis, K. Farrell, in: F.W. Wiffen, J.A. Spitznagel (Eds.), Advanced Techniques for Characterizing Microstructures, AIME, New York, 1982, p. 487.
[18] W.C. Oliver, G.M. Pharr, J. Mater. Res. 7 (1992) 1564.
[19] L.E. Samuels, T.O. Mulhearn, J. Mech. Phys. Solids 5 (1957) 125.
[20] E.H. Lee, J.D. Hunn, T.S. Byun, L.K. Mansur, J. Nucl. Mater. 280 (2000) 18.
[21] H. Ullmaier, Nucl. Fus. 24 (1984) 1073.
[22] E.P. EerNisse, S.T. Picraux, J. Appl. Phys. 48 (1977) 9.
[23] G.M. McCracken, Rep. Progr. Phys. 38 (1975) 317.
[24] K.L. Wilson, in: Data Compendium for Plasma–Surface Interactions, Nuclear Fusion Special Issue 1984, International Atomic Energy Agency, Vienna, 1984, pp. 85–94.
[25] L.K. Mansur, J. Nucl. Mater. 216 (1994) 97.